Talanta 257 (2023) 124217

Contents lists available at ScienceDirect

Talanta

journal homepage: www.elsevier.com/locate/talanta

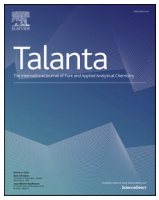

Ultra-precise weak measurement-based interfacial biosensors

Lizhong Zhang [a,b,1], Qiang Huang [a,c,d,1], Xiaonan Zhang [a,e], Zhen Zeng [a,b], Hailong Zhang [f,g], Tian Guan [a,e], Yang Xu [a,b], Chongqi Zhou [a,h], Lingqin Meng [a,b], Gengyu Liang [a,b], Zhangyan Li [a,h], Bei Wang [a,b], Le Liu [i], Cuixia Guo [j,**], Yonghong He [a,b,*]

[a] Institute of Optical Imaging and Sensing, Shenzhen Key Laboratory for Minimal Invasive Medical Technologies, Tsinghua Shenzhen International Graduate School, Tsinghua University, Shenzhen, 518055, China
[b] Institute of Biopharmaceutical and Health Engineering, Tsinghua Shenzhen International Graduate School, Tsinghua University, Shenzhen, 518055, China
[c] Shenzhen Shengqiang Technology Co., Ltd, China
[d] Tsinghua Shenzhen International Graduate School, Tsinghua University, Shenzhen, 518055, China
[e] School of Medicine, Tsinghua University, Beijing, 100084, China
[f] Key Laboratory of Photonic Control Technology (Tsinghua University), Ministry of Education, Beijing, 100084, China
[g] Department of Precision Instrument, Tsinghua University, Beijing, 100084, China
[h] Department of Physics, Tsinghua University, Beijing, 100084, China
[i] Institute of Materials Research, Shenzhen International Graduate School, Tsinghua University, Shenzhen, 518055, China
[j] School of Mechanical Engineering and Automation, Fuzhou University, Fuzhou, 350108, China

ARTICLE INFO

Handling Editor: Prof. J.-M. Kauffmann

Keywords:
Weak measurements
Biosensors
Self-referencing
Ultra-precision
Refractive index sensing

ABSTRACT

In this study, an interfacial biosensing scheme with ultra-precision is proposed. The scheme uses weak measurement techniques to ensure ultra-high sensitivity of the sensing system while improving the stability of the system through self-referencing and pixel point averaging, thus achieving ultra-high detection accuracy of biological samples. In specific experiments, we have used the biosensor in this study to perform specific binding reaction experiments for protein A and Mouse IgG with a detection line of 2.71 ng/mL for IgG. In addition, the sensor is non-coated, simple in structure, easy to operate, and low in cost of use.

1. Introduction

Life is the eternal theme of scientific research, and since the new century, life science research has been on the rise, with a series of huge breakthroughs that are making a real difference in human life. At the same time, the field of biosensors, formed by the intersection of life sciences and multiple disciplines, has also burst forth with amazing vitality. Biosensors are generally combined with specific enzymes, antibodies, antigens, proteins, nucleic acids, small molecules, and other biologically active analytes through sensitive materials, which are converted into distinguishable electrical, optical, and thermal properties through a physicochemical transducer, and then converted into quantifiable electrical signals through amplification [1]. Amongst other things, the optical signal has the advantages of high sensitivity, resistance to external interference, good stability, and low noise compared to other physical signals [2,3]. As a result, optical biosensors have shown good performance in bio-detection systems and have contributed to huge breakthroughs in scientific research and industry in biomedicine, food and health, material characterization, drug development, medical devices, and environmental protection.

Optical biosensors with evanescent fields to sense target objects and environmental media make up a major part of optical biosensors due to their non-marking and non-invasive advantages. The two main types of evanescent field biosensors currently available are total internal reflection sensors and surface plasmon resonance sensors. However, the rather smooth phase response limits the resolution of total internal reflection sensors for high sensitivity detection of biomolecular interactions; SPR sensors, while offering better resolution, the precise control of gold film thickness and the optimization of incidence angle and wavelength cause operational complexity and cost of use [4–8].

* Corresponding author. Tsinghua Shenzhen International Graduate School, Tsinghua University, Shenzhen 518055, China.
** Corresponding author.
E-mail addresses: guocx@fzu.edu.cn (C. Guo), heyh@sz.tsinghua.edu.cn (Y. He).
[1] These authors contributed equally to this work and should be considered co-first authors.

https://doi.org/10.1016/j.talanta.2022.124217
Received 22 September 2022; Received in revised form 17 December 2022; Accepted 21 December 2022
Available online 22 December 2022

Since its introduction in 1988, weak measurement techniques have shown great advantages in the field of high-precision measurement [9–11]. In particular, the proposal of frequency domain weak measurement systems and the implementation of weak measurement sensing systems with universal value have allowed weak measurement sensors to demonstrate excellence in the field of bio-detection. Based on the weak measurement technology's advantages and evanescent field sensing characteristics, we have implemented several sets of weak measurement-based interfacial biosensors to achieve high-precision biological information acquisition at common glass interfaces [12–15].

In sensor development, sensitivity (S) and detection limit (DL) are important parameters that define the performance of a biosensor. Sensitivity, which refers to the strength of the light-matter interaction, is the change in amplitude of the transduction signal in response to any change in the analyte. DL is defined as the minimum detectable amount of the analyte, determined by the resolution of the readout system. DL = δ/S where δ and S are the noise and sensitivity in the transduction signal respectively, and therefore a balance between sensitivity and stability of the system is required in development. The application of weak measurement techniques has greatly improved the sensitivity of sensing systems, so improving sensor anti-interference is particularly important to improve the performance of weak measurement biosensors. Interfacial biosensors are susceptible to external factors such as temperature and vibration. Self-referencing in sensors is both necessary and important, as well as a means of resolving external disturbances. The implementation of a weak measurement-based interfacial refractive index imaging sensor in previous work establishes a solid basis for our proposal of a self-referencing weak measurement-based interfacial biosensor. We build two channels within the same interface without the need to add expensive additional detection elements. We differentiate the signals acquired in the experimental and reference channels to achieve noise reduction, and we further improve the stability of the system by averaging the pixel points corresponding to the examined areas in each of the two channels on the CCD.

In this work, a self-referencing interfacial biosensing system based on weak measurement techniques is proposed for the first time and enables the study of biomolecular interactions. In our work, we have developed an interfacial weak measurement biosensing system with ultra-high detection accuracy by ensuring the stability of the system through differential and pixel averaging methods while ensuring that the sensor has extremely high sensitivity through the weak measurement technique. The sensor has a detection accuracy of 2.71 ng/mL for IgG. In addition, the sensor in this study is characterized by the simple structure, high robustness, wide range of applications, low detection cost, and easy system and experimental operation of common optical sensors.

2. Material and methods

2.1. Material

Phosphate buffered solution (PBS, powder) and the albumin bovine V (BSA) were purchased from Solarbio Science & technology company (Beijing, China). PBS at pH 7.3 with a concentration of 0.01 M/L provides an environment for biomolecular interactions. Dopamine hydrochloride and Tris (hydroxymethyl)aminomethane (TRIS) were provided by Aladdin (Shanghai, China). Prepare a solution of dopamine hydrochloride at a concentration of 1 mg/mL dissolved in TRIS solution at a concentration of 10 mM/L and store it away from light. Recombinant Protein A and Mouse immunoglobulin G (Mouse IgG) were purchased from Bioss (Beijing, China). No protein blocking solution, 2% was purchased from Sangon Biotech (Shanghai, China).

2.2. Methods

As shown in Fig. 1, the light emitted by the superluminescent diode is collimated through a collimating lens. The collimated light passes through a front-selective polarizer and achieves total internal reflection on the inner surface of the prism of the HZF6, causing a phase difference between the P and S polarizations. The collimated light then passes through a super achromatic quarter wave plate, which converts the phase difference into a spin. Finally, the collimated light, after passing through a quartz rotator and a post-selective polarizer, is imaged by an imaging lens that images the total internal reflection interface onto a CCD. As shown in Fig. 1, we coupled the prismatic total internal reflection interface with a flow channel machined using 3D printing technology, and in this project, we set up two flow channels - an experimental flow channel and a reference flow channel. The runner and the prism together form the 'chip' unit of the sensor. In the specific experiments, we add reactants to the experimental flow channel in sequence and continuously add standard solutions to the reference flow channel (we generally choose deionized water, sodium chloride solution or PBS as the standard solution depending on the detection scenario), during the reaction process we differential the signals from the experimental and reference channels collected by the system to achieve biodetection. According to the weak value amplification principle proposed by AAV, diagrams P1, C–W-R, P2 in Fig. 1 serve as the three core components of pre-selection, the weak interaction, and post-selection for weak measurements, respectively. We describe the theoretical basis of the above implementation in detail in the SI

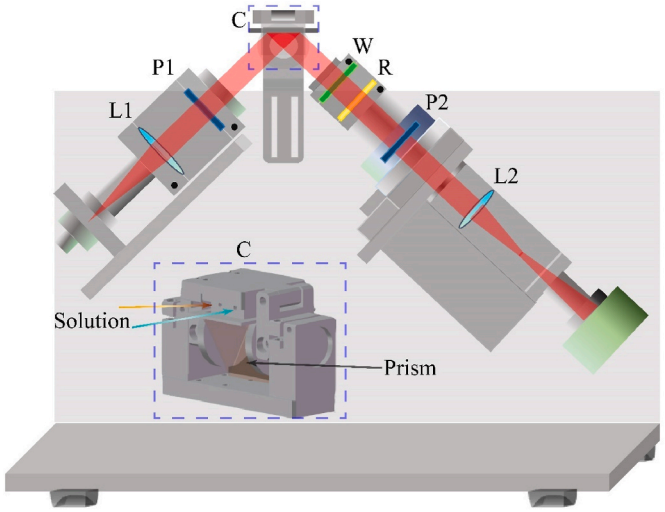

Fig. 1. Overview of the instrument. L1 is a collimated lens, L2 is an imaging lens, P1 and P2 are line polarizers, W is a quarter wave plate and R is an optical rotator. C is the structure where light is coupled with the system to be measured. The axonometric view of C is given in the inset. And it's easy to replace the prism and the 'chip'.

3. Results and discussion

The prism-based elements used as sensor 'chip' units in this project are partly due to the low cost of glass and partly because the glass surface modification process has been widely used for the preparation of biomolecular-level sensors. However, the refractive index of the glass is sensitive to external temperature. Changes in external temperature can introduce large errors in the system.

To confirm the perturbation of the 'chip' by temperature changes, we simulate the heat transfer process using COMSOL software. The effect of temperature changes on the refractive index of the 'chip' is simulated by varying the initial temperature of the fluid in the flow channel (below and above room temperature). As shown in Fig. 2, when a liquid different from room temperature enters the system through the flow channel, the refractive index near the inner surface of the prism fluctuates significantly and introduces a refractive index error; the temperature of the 'chip' at room temperature converges to room

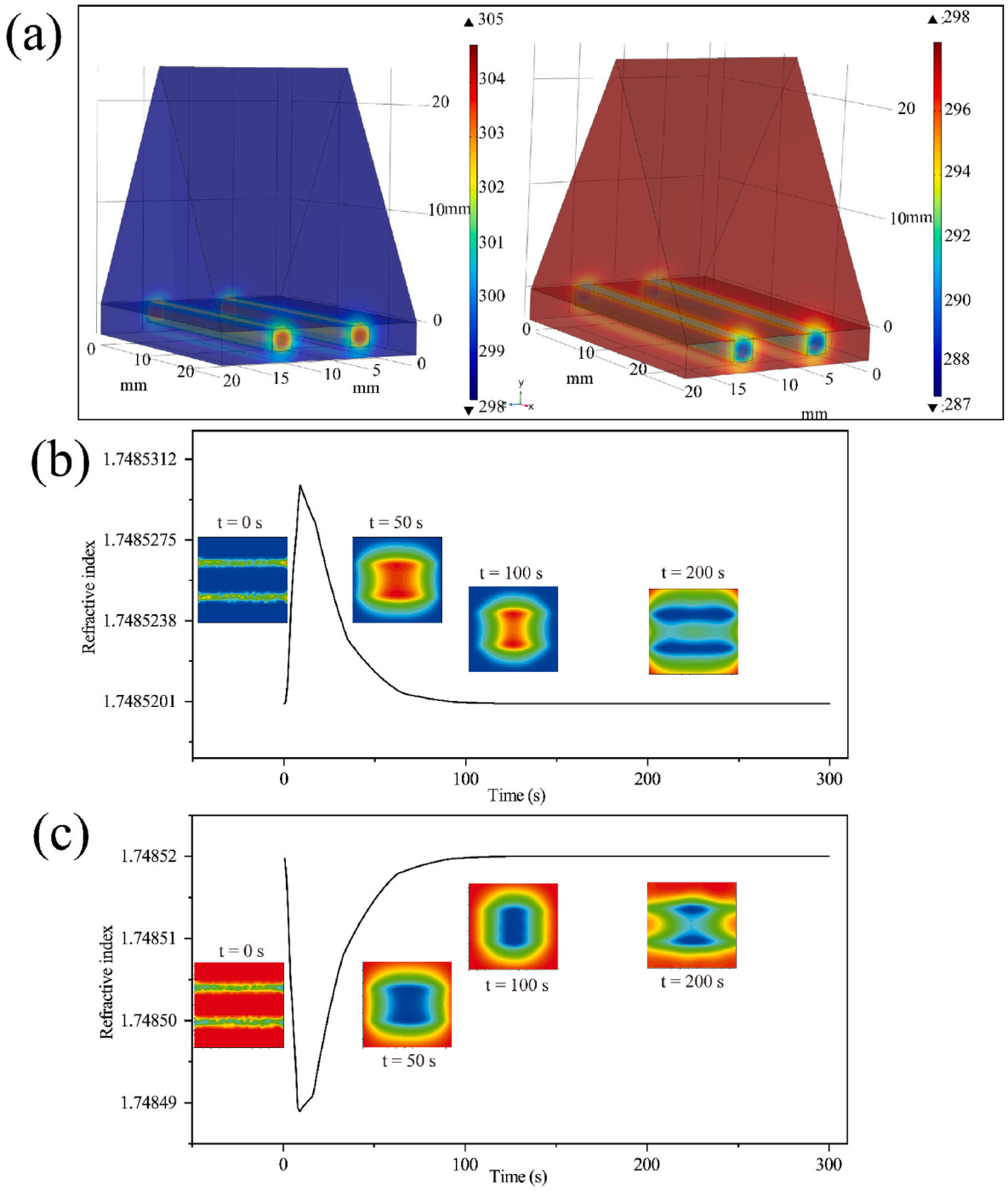

Fig. 2. (a) Simulation of heat conduction process in 'chip' and prism. (b) The curve is the refractive index change in the spot region during the cooling of high-temperature liquids. The insets show the refractive index distribution of the sensing interface at different moments. (c) The curve is the refractive index change in the spot region during the warming of low-temperature liquids. (More detailed simulation images are available in the supplementary file.)

temperature, but the error introduced in the sensor during this process is not eliminated. At the same time, maintaining a stable refractive index within the prism after temperature convergence and resisting interference from other factors can cause temperature changes to remain a challenge.

In order to verify the robustness of the sensors proposed in this project to temperature, we evaluated them by passing deionized water through the flow channel at room temperature, which is different from the room temperature. In the experiments, the temperature variation was scaled up in order to demonstrate more clearly the sensor's resistance to external temperature variations. In Fig. 3(a–b), each channel of the sensor is shown, as well as the signal variation curve after differencing the two channels. Here each channel can be seen as a separate conventional interface weak measurement sensor. As shown in Fig. 3 (a–b), when deionized water different from room temperature is passed into the flow channel and becomes room temperature in the flow channel, we have significant changes in the signals collected at the receiving end, i.e., the sensor chip is very sensitive to temperature perturbations; whereas, as a self-referencing scheme proposed in this project, there are no significant changes in the signals collected at the receiving end after differencing the two channels. This also demonstrates the good robustness of the sensor system in this study to

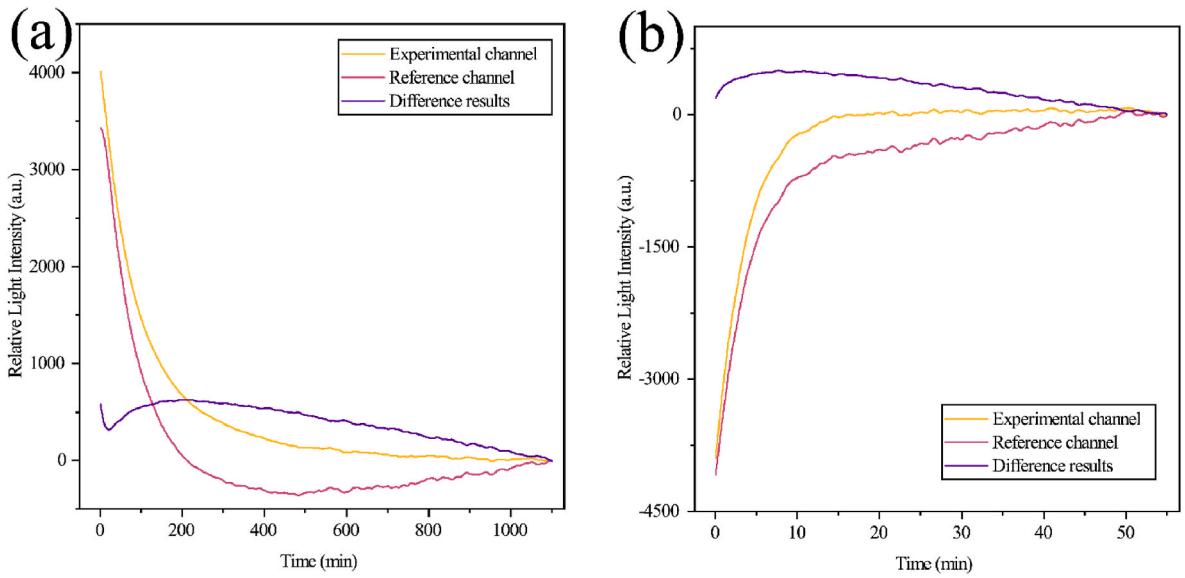

Fig. 3. (a) The relative light intensity of two channel and the differential results from 312.75 K to 302.85 K. (b) The relative light intensity of two channels and the differential results from 283.25 K to 295.45 K.

temperature variations.

We also further improve the stability of the system by averaging the pixel points. As shown in Fig. 4, we compare the variance of the sensor fluctuations over 20 min after averaging the pixel points in each of the eight regions, such as Area 1, in turn. As shown in Fig. 4(b), the variance decreases as the number of pixel points increases and the variance fluctuation of the system stabilize at 11.7 over 20 min when the average pixel point is greater than 1024. This also provides us with a reference for the minimum range per detection point when combining the system with microfluidics in the future.

To further validate the sensing ability of the sensors in this study in biomolecular interactions, we performed an IgG to protein A specific binding reaction assay. Taking advantage of the ease with which silica can be surface functionalized, we first modified the surface of the 'chip' using dopamine in the experimental channel (dopamine self-polymerizes to form a thin, surface-adhesive film that can be used for surface modification with a variety of organic and inorganic materials), and then sequentially coated and sealed the surface of the 'chip' using protein A solution with a concentration of 100 μg/mL and protein-free sealant. The functionalized 'chip' surface is then encapsulated and sealed with protein A and protein-free sealing solutions, followed by the sequential passage of different concentrations of IgG solutions. While the experimental channel is being treated, the reference channel is continuously fed with PBS solution, which is used for noise reduction by self-reference. Fig. 5(a) shows the results after the two channels have been differenced. As shown in Fig. 5(b), IgG solutions with

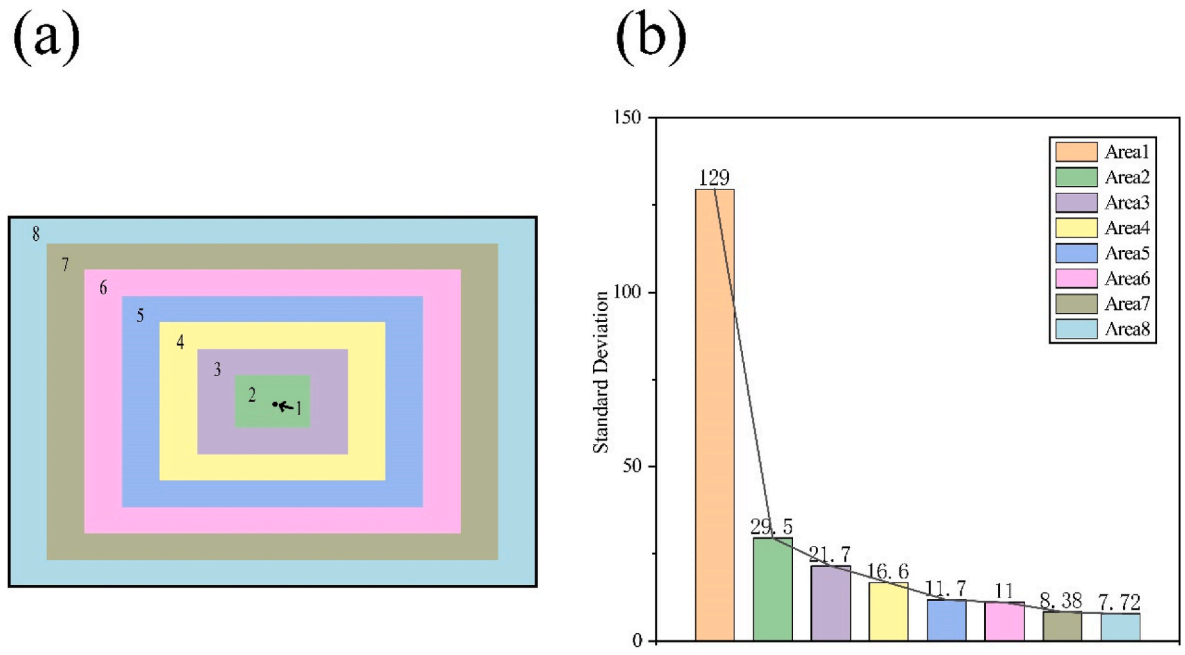

Fig. 4. (a) This is a schematic diagram of 7 concentric rectangular regions with different areas taken at the center of point 1. The area of these regions from 1 to 8 are 1, 16, 64, 256, 1024, 16,384, 65,536, and 102,400. (b) This is the distribution of the standard deviation of the pixel values over 20 min for 8 different areas. Area 1 in the diagram represents point 1 in (a), and other areas.

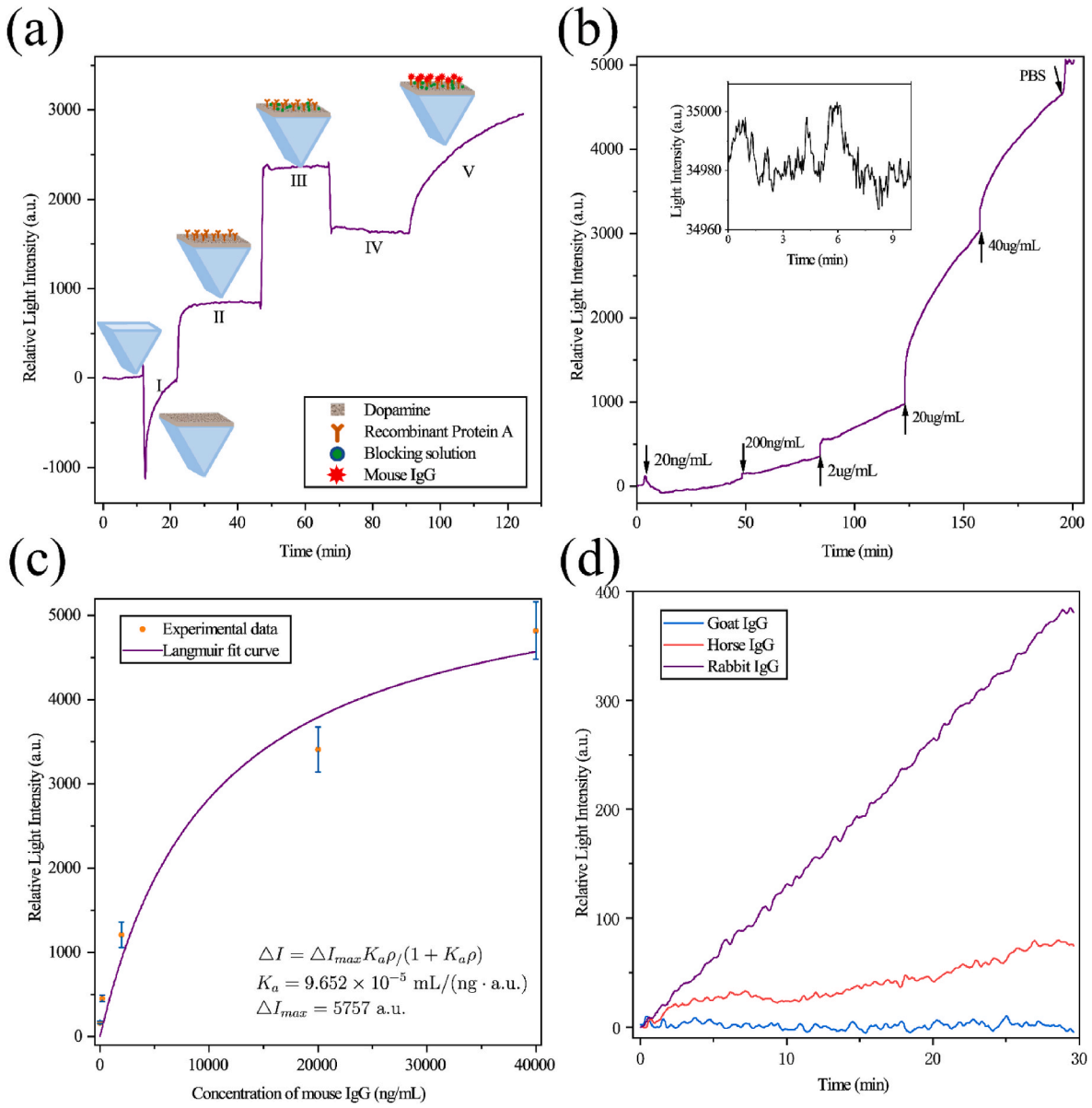

Fig. 5. (a) Relative light intensity changes during the experiment after difference. I Dopamine- 'Chip' functionalized; II Protein A- 'Chip' encapsulated; III Protein-free sealant- 'Chip' sealed; IV PBS-Baseline; V Mouse IgG-Molecular interaction. (b) Changes in relative light intensity at different concentrations of IgG. The inset shows in light intensity of a 20 g/L NaCl solution over 10 min, with a standard deviation of 7.72. (c) Langmuir adsorption model fits the experimental results. K_a is the absorption constant, ρ is the concentration of IgG, and ΔI is the relative light intensity change caused by the specific binding reaction. (d) Relative light intensity caused by different target samples using goat anti-rabbit IgG as probe layer. (The figure about relative light intensity caused by mouse IgG using different targets is in the supplementary file.)

concentrations of 0.02ug, 0.2ug, 2ug, 20ug, and 40ug caused a change in the light intensity of the acquired signal as 172 a. u., 430 a. u., 1051 a. u., 3111 a. u., 4726 a. u., respectively. Also, the detection limit of the system for IgG can be calculated as 2.71 ng/mL based on the system fluctuations in the previous section and the equation $c_L = 3 \times \sigma_s / (\Delta I / \Delta c)$, c_L is the detection limit, σ is the standard deviation at system stability, ΔI is the change of light intensity for Δc which is the change of the concentration of IgG In Fig. 5(c), we applied the Langmuir adsorption model to fit the experimental results. As shown in Fig. 5(c), the absorption constant was calculated as 9.652 × 10-5 mL/(ng·a.u.). As shown in Table 1, we compared the accuracy of IgG detection by different interfacial sensors, and the sensor in this study has a clear advantage in terms of detection accuracy compared to the results in other reported literature.

In order to verify the specific binding ability of the sensor, the PBS,

Table 1
IgG detection limits in different methods.

Method	Detection limit of IgG
Low-Coherence Spectral-Domain Interferometer [16]	110 ng/mL
Weak measurement system with common path [17]	1000 ng/mL
SPR based on TFBG [18]	500 ng/mL
SPR based on PDA-ZnO@Au [19]	37.5 ng/mL
SPR based on hollow gold nanospheres [20]	19 ng/mL
TIR ellipsometry based SPR [21]	45 ng/mL
Liquid crystal microdroplets [22]	16 ng/mL
Extended-Gate Type organic field effect transistor [23]	620 ng/mL
Optofluidic point-of-care testing fluorescence [24]	12.5 ng/mL
Self-referencing interfacial weak measurement biosensor	2.71 ng/mL (this work)

BSA, and IgG solutions were tested using the encapsulated and sealed 'chip'. As shown in Fig. 5 (d), there was no significant signal change in the sensing system when the samples were PBS and BSA, while the sensing system picked up significant signal changes when the samples were IgG. In summary, the results show that the sensor proposed in this project is capable of achieving ultra-high accuracy and specificity in the identification of biomolecules.

4. Conclusion

In this study, we have combined a self-referencing approach with weak measurement techniques to achieve an interfacial biosensor on a common glass 'chip' with ultra-high detection accuracy. The use of self-referencing and pixel averaging improves the stability of the system while using weak measurement techniques to maintain the high sensitivity of the system, and the simplicity of the structure and the lack of surface coating allows it to be coupled to a wide range of optical systems. In specific experiments, we demonstrate the immunity of the self-referencing sensor in this study compared to conventional sensing systems. In experiments on biomolecular interactions, the system achieves a detection accuracy of 2.71 ng/mL for IgG, which is one order of magnitude higher than that of other interfacial sensing systems. This study proposes a strategy to improve the detection accuracy of interfacial biosensors, which can be applied to all types of sensors in order to improve performance.

Credit author statement

Lizhong Zhang: Writing - Original Draft, Investigation Qiang Huang: Software, Validation Xiaonan Zhang: Formal analysis Zhen Zeng: Visualization Hailong Zhang: Data Curation Tian Guan: Conceptualization Yang Xu: Writing - Original Draft Chongqi Zhou: Methodology Lingqin Meng: Resources Gengyu Liang: Validation, Resources Zhangyan Li: Visualization Bei Wang: Conceptualization Le Liu: Writing - Review & Editing Cuixia Guo: Project administration, Writing - Review & Editing. Yonghong He: Project administration, Funding acquisition, Supervision.

Declaration of competing interest

The authors declare that they have no known competing financial interests or personal relationships that could have appeared to influence the work reported in this paper.

Data availability

The data that has been used is confidential.

Acknowledgments

This work was made possible with the financial support from National Natural Science Foundation of China (NSFC) (61875102 and 62105068), Science and Technology Research Program of Shenzhen City (JCYJ20200109110606054 and WDZC20200821141349001).

Appendix A. Supplementary data

Supplementary data to this article can be found online at https://doi.org/10.1016/j.talanta.2022.124217.

References

[1] X.D. Fan, I.M. White, S.I. Shopova, H.Y. Zhu, J.D. Suter, Y.Z. Sun, Sensitive optical biosensors for unlabeled targets: a review, Anal. Chim. Acta 620 (1–2) (2008) 8–26, https://doi.org/10.1016/j.aca.2008.05.022.
[2] L.C. Clark, C. Lyons, Electrode systems for continuous monitoring in cardiovascular surgery, Ann. N. Y. Acad. Sci. 102 (1) (1962) 29–&, https://doi.org/10.1111/j.1749-6632.1962.tb13623.x.
[3] A.E. Goodling, S. Nagelberg, B. Kaehr, C.H. Meredith, S.I. Cheon, A.P. Saunders, M. Kolle, L.D. Zarzar, Colouration by total internal reflection and interference at microscale concave interfaces, Nature 566 (7745) (2019) 523, https://doi.org/10.1038/s41586-019-0946-4.
[4] W. Wang, Y. Yang, S. Wang, et al., Label-free measuring and mapping of binding kinetics of membrane proteins in single living cells, Nat. Chem. 4 (2012) 846–853, https://doi.org/10.1038/nchem.1434.
[5] A.M. Armani, R.P. Kulkarni, S.E. Fraser, R.C. Flagan, K.J. Vahala, Label-free, single-molecule detection with optical microcavities, Science 317 (5839) (2007) 783–787, https://doi.org/10.1126/science.1145002.
[6] P. Zhang, G. Ma, W. Dong, et al., Plasmonic scattering imaging of single proteins and binding kinetics, Nat. Methods 17 (2020) 1010–1017, https://doi.org/10.1038/s41592-020-0947-0.
[7] G. Ma, Z. Wan, Y. Yang, et al., Optical imaging of single-protein size, charge, mobility, and binding, Nat. Commun. 11 (2020) 4768, https://doi.org/10.1038/s41467-020-18547-w.
[8] E.A. Smith, W.D. Thomas, L.L. Kiessling, R.M. Corn, Surface plasmon resonance imaging studies of protein-carbohydrate interactions, J. Am. Chem. Soc. 125 (20) (2003) 6140–6148, https://doi.org/10.1021/ja034165u.
[9] Y. Aharonov, D.Z. Albert, L. Vaidman, How the result of a measurement of a component of the spin of a spin-1/2 particle can turn out to Be 100, Phys. Rev. Lett. 60 (14) (1988) 1351–1354, https://doi.org/10.1103/PhysRevLett.60.1351.
[10] N.W.M. Ritchie, J.G. Story, R.G. Hulet, Realization of a measurement of a weak value, Phys. Rev. Lett. 66 (9) (1991) 1107–1110, https://doi.org/10.1103/PhysRevLett.66.1107.
[11] O. Hosten, P. Kwiat, Observation of the spin Hall effect of light via weak measurements, Science 319 (5864) (2008) 787–790, https://doi.org/10.1126/science.1152697.
[12] L.P. Xu, L. Luo, H. Wu, Z.C. Luo, Z.Y. Zhang, H.F. Shi, T.Y. Chang, P. Wu, C.L. Du, H.L. Cui, Measurement of chiral molecular parameters based on a combination of surface plasmon resonance and weak value amplification, ACS Sens. 5 (8) (2020) 2398–2407, https://doi.org/10.1021/acssensors.0c00346.
[13] N. Brunner, C. Simon, Measuring small longitudinal phase shifts: weak measurements or standard interferometry? Phys. Rev. Lett. 105 (1) (2010).
[14] Y. Xu, L.X. Shi, T. Guan, C.X. Guo, D.M. Li, Y.X. Yang, X.N. Wang, L.Y. Xie, Y.H. He, W.Y. Xie, Optimization of a quantum weak measurement system with its working areas, Opt Express 26 (16) (2018) 21119–21131, https://doi.org/10.1364/Oe.26.021119.
[15] Y. Xu, C.Q. Zhou, L.X. Shi, X.N. Zhang, T. Guan, C.X. Guo, Z.Y. Li, X.H. Xing, Y. H. Ji, L. Liu, Y.H. He, Imaging sensor for the detection of the flow battery via weak value amplification, Anal. Chem. 93 (38) (2021) 12914–12920, https://doi.org/10.1021/acs.analchem.1c02189.
[16] C.X. Guo, X.J. Yang, Z.Y. Shen, J.P. Wu, S.Y. Zhong, Y.H. He, T. Guan, F.Y. Chen, A fluidic biosensor based on a phase-sensitive low-coherence spectral-domain interferometer, Sensors 18 (11) (2018).
[17] Y.L. Zhang, D.M. Li, Y.H. He, Z.Y. Shen, Q.H. He, Optical weak measurement system with common path implementation for label-free biomolecule sensing, Opt. Lett. 41 (22) (2016) 5409–5412, https://doi.org/10.1364/Ol.41.005409.
[18] Q. Wang, J.Y. Jing, B.T. Wang, Highly sensitive SPR biosensor based on graphene oxide and staphylococcal protein A Co-modified TFBG for human IgG detection, IEEE Trans. Instrum. Meas. 68 (9) (2019) 3350–3357, https://doi.org/10.1109/Tim.2018.2875961.
[19] H. Yang, X. Zhao, Z. Zhang, P. Ma, X. Wang, D. Song, Y. Sun, Biotin-streptavidin sandwich integrated PDA-ZnO@Au nanocomposite based SPR sensor for hIgG detection, Talanta 246 (2022), 123496, https://doi.org/10.1016/j.talanta.2022.123496.
[20] S. Li, Q. Wu, P. Ma, Y. Zhang, D. Song, X. Wang, Y. Sun, A sensitive SPR biosensor based on hollow gold nanospheres and improved sandwich assay with PDA-Ag@Fe3O4/rGO, Talanta 180 (2018) 156–161, https://doi.org/10.1016/j.talanta.2017.12.051.
[21] U. Pant, S. Mohapatra, R.S. Moirangthem, Total internal reflection ellipsometry based SPR sensor for studying biomolecular interaction, Mater. Today Proc. 28 (2020) 254–257, https://doi.org/10.1016/j.matpr.2020.01.602.
[22] K. Lee, K.C. Gupta, S.Y. Park, I.K. Kang, Anti-IgG-anchored liquid crystal microdroplets for label free detection of IgG, J. Mater. Chem. B 4 (4) (2016) 704–715, https://doi.org/10.1039/c5tb02131f.
[23] T. Minamiki, T. Minami, R. Kurita, O. Niwa, S. Wakida, K. Fukuda, D. Kumaki, S. Tokito, A label-free immunosensor for IgG based on an extended-gate type organic field effect transistor, Materials 7 (9) (2014) 6843–6852, https://doi.org/10.3390/ma7096843.
[24] D. Song, J.Y. Liu, W.J. Xu, X.Z. Han, H.L. Wang, Y. Cheng, Y.X. Zhuo, F. Long, Rapid and quantitative detection of SARS-CoV-2 IgG antibody in serum using optofluidic point-of-care testing fluorescence biosensor, Talanta 235 (2021).